Available online at www.sciencedirect.com
SCIENCE DIRECT®
Journal of Solid State Chemistry 178 (2005) 3243–3250
JOURNAL OF SOLID STATE CHEMISTRY
www.elsevier.com/locate/jssc

Mechanosynthesis of zinc ferrite in hardened steel vials: Influence of ZnO on the appearance of Fe(II)

Thomas Verdier, Virginie Nachbaur, Malick Jean*

Institut des Matériaux, Université de Rouen, LASTSM, BP12 76801 Saint Etienne du Rouvray, Cedex, France

Received 8 April 2005; received in revised form 7 July 2005; accepted 31 July 2005
Available online 9 September 2005

Abstract

Nanocrystalline $ZnFe_2O_4$ spinel powders are synthesized by high-energy ball milling, starting from a powder mixture of hematite (α-Fe_2O_3) and zincite (ZnO). The millings are performed under air using hardened steel vials and balls. X-ray diffraction and Mössbauer spectrometry are used to characterize the powders. A spinel phase begins to appear after 3 h of milling and the synthesis is achieved after 9 h. Phase transformation is accompanied by a contamination due to iron coming from the milling tools. A redox reaction is also observed between Fe(III) and metallic iron during milling, leading to a spinel phase containing some Fe(II). The mechanism for the appearance of this phase is studied: ZnO seems to have a non-negligeable influence on the synthesis, by creating an intermediate wüstite-type phase solid solution with FeO.

Keywords: Mechanosynthesis; Zinc ferrite; Mössbauer Spectrometry; Wüstite-type phase

1. Introduction

Spinel ferrites crystallize to a cubic closed-pack structure of oxygen ions in which tetrahedral (A) and octahedral (B) sites are occupied by cations. They have the general formula $(M_{1-\lambda}Fe_\lambda)_A(M_\lambda Fe_{2-\lambda})_BO_4$ where M represents a metal cation and λ is the inversion parameter. λ is 1 for a perfectly inverse spinel, 2/3 for the random arrangement and 0 for a perfectly normal spinel. $ZnFe_2O_4$ is usually identified as a normal spinel when it is synthesized by ceramic way with the formula $(Zn^{2+})_A(Fe^{3+}Fe^{3+})_BO_4$ [1].

These compounds are widely used for their technological applications, which are essentially their magnetic and catalytic properties. Zinc ferrite presents a high interest as an absorbent for desulfurization of hot coal gas, capable of removing hydrogen sulfide [2], but it also can be used as an starting materials for obtaining substituted ferrites with particular magnetic characteristics. In both cases, the syntheses with new methods may allow to improve their properties and their use [3]. For example, high-energy ball milling leads to a change in the distribution of cations in both sites, resulting in an increase of magnetic properties [4].

Indeed, mechanosynthesis of ferrites usually leads to nanometric powders with structural properties deviating from the ceramic compound. In particular, cation distribution is characterized by an inversion phenomenon in ferrites which are known as normal [5,6] and/or by the apparition of unexpected iron valencies [7].

Indeed, we observed Fe^{2+} cations in the spinel structure even though only Fe_2O_3 and ZnO are introduced in the vials [7]. We also observed that the obtained structure depends on the choice of the rotation speeds of the vials and the main disk, which defines milling modes. In the present study, we try to elucidate the formation of Fe^{2+} leading to zinc-substituted magnetites obtained with one of the milling modes.

*Corresponding author. Fax: +33 2 32 95 50 72.
E-mail address: malick.jean@univ-rouen.fr (M. Jean).

0022-4596/$ - see front matter © 2005 Elsevier Inc. All rights reserved.
doi:10.1016/j.jssc.2005.07.033

2. Experimental

Millings are performed under air in a high-energy planetary mill (Vario-Mill, Fritsch) using tempered steel vials (80 mL) and steel balls. Initial powders are hematite (α-Fe_2O_3) and zincite (ZnO) obtained from Alfa Aesar (99% purity or better). Particle sizes are observed by scanning electron microscopy. Their size range are between 150 and 500 nm for zincite and between 100 and 300 nm for hematite. We use 5 new balls of 15 mm of diameter for each milling and 3.455 g of powder. In this conditions the ball-to-powder weight ratio is 20. The velocities are 500 r.p.m. for the main disk, −500 r.p.m. for the vials.

The samples are called ZnFe*t* where *t* is the milling duration (in hours), a letter a, b or c may follow to denote several trials. The notation ZnFecera is used for the ceramic zinc ferrite.

X-ray powder diffraction (XRD) analysis is performed on a Siemens D5000 diffractometer, using Co $K\alpha$ radiations ($\lambda_{K\alpha1} = 0.178897$ and $\lambda_{K\alpha2} = 0.179285$ nm). Diffraction intensity is measured in the 2θ range between 20° and 90°, with a 2θ step of 0.03° for 8 s per point. X-ray diffraction line broadening is influenced by the microstructure of the solid, i.e., size and morphology of crystallites (coherently diffracting domains) and imperfections (for example, microstrains, stacking faults, etc.). In order to obtain these parameters, peak profiles are modeled with pseudo-Voigt functions [8]. Pattern decomposition is carried out by means of the profile fitting program Winplotr [9]. After correcting data from instrumental effects, the microstructure is studied using the XRD profile analysis described by Langford [10].

Mössbauer measurements are performed at room temperature using a constant acceleration spectrometer and a ^{57}Co/Rh source, which is calibrated relative to α-Fe. Hyperfine parameters are given using the following notation: DI for isomer shift, Δ for quadripole spilitting, ε for quadripole shift and B for magnetic hyperfine field.

3. Results and discussion

3.1. X-ray diffraction analysis

After 3 h of grinding, X-ray diffraction pattern (Fig. 1) shows a decrease in peak intensities of ZnO and α-Fe_2O_3, whereas peaks attributed to a spinel phase appear. The intensity ratio of 100(ZnO)/104(Fe_2O_3), which was 0.8 before grinding, is almost 0, indicating that zinc oxide becomes rapidly amorphous compared to α-Fe_2O_3. It has already been observed that the size of ZnO seems to be a critical parameter, it must reach 7 nm before the appearance of a spinel phase [11].

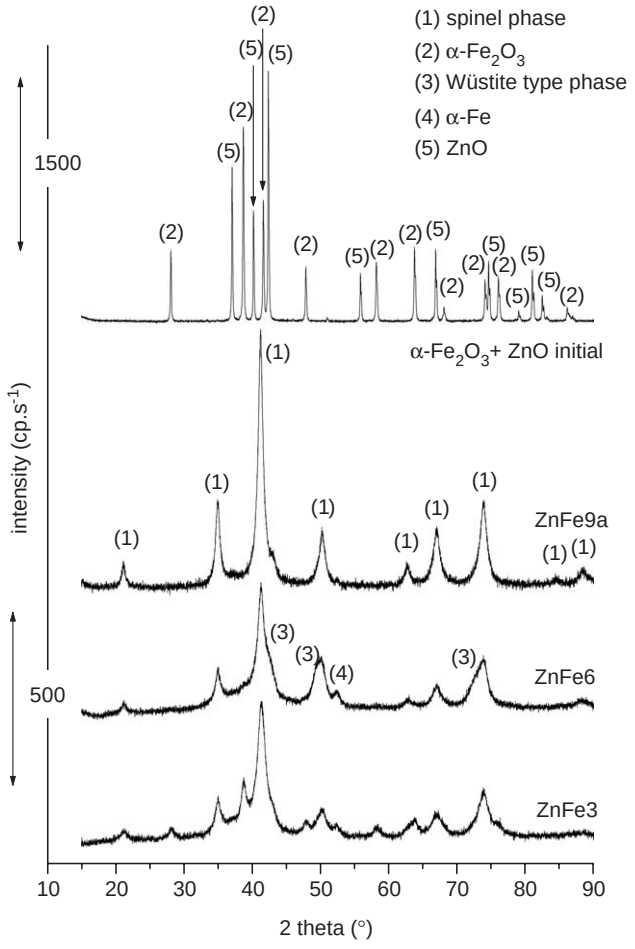

Fig. 1. X-ray powder diffraction patterns of ball-milled ZnO–α-Fe_2O_3 mixture.

After 6 h of grinding (Fig. 1), the peaks of hematite have almost disappeared, the spinel phase is still observed and a new phase is found, identified as a cubic wüstite-type phase.

After 9 h of grinding (Fig. 1), the spinel phase is pure excepting one peak of metallic iron. This peak is also observed for the 6 h grinding, and its origin is the abrasion of the balls and vials made of tempered steel.

The 9 h milling has been performed three times (ZnFe9a, b and c) and no noticeable difference between X-ray diffraction patterns has been observed.

For a prolonged grinding time (24 h), the X-ray pattern is identical to the 9 h pattern.

The results of cell parameter and crystallite size are provided in Table 1. For comparison, the cell parameters of JCPDS file no. 22-1012 and this of a ceramic zinc ferrite are also reported.

Cell parameters and crystallite size are very similar for the four samples, indicating a good reproducibility of the millings, and showing that increasing the time of milling has no noticeable influence. The cell parameters are slightly less than that of JCPDS file and than that of ceramic zinc ferrite.

Table 1
Cell parameters and crystallites sizes for pure spinel phase

Sample	Cell parameter (nm)	Size (nm)
ZnFe9a	0.8438±0.0001	11.3±0.5
ZnFe9b	0.8438±0.0001	11.1±0.5
ZnFe9c	0.8437±0.0001	10.9±0.5
$ZnFe2_4$	0.8437±0.0001	10.5±0.5
ZnFecera	0.84431±0.00001	—
JCPDS 22-1012	0.84411	—

For O'Neill [12], on compounds obtained by ceramic route with inversion parameters λ lower than 0.2, the cell parameter decreases with λ according to the following equation: a (nm) = 0.84423–0.001247λ.

To our knowledge, Ermakov et al. [6] reported for the first time that the effect of a high-energy ball milling on zinc ferrite is a change in the structure of zinc ferrite (normal to inverse). Same results have been obtained later by Sepelak [5,13], who observed that this inversion leads to a contraction of the crystal lattice from 0.84432 (ceramic sample) to 0.84136 nm (same sample milled for 24 min). The same authors report that the structure of zinc ferrite obtained by mechanosynthesis from ZnO and α-Fe_2O_3 is close to that of milled $ZnFe_2O_4$ [14].

Based on the only X-ray diffraction results, it is hazardous to conclude to an inversion phenomenon. Actually, Li et al. [15] have determined an inversion parameter of 0.6 by Mössbauer spectroscopy on a milled $ZnFe_2O_4$ without observing any decrease in the cell parameter (initial: 0.8442 nm, after milling: 0.8440 nm). Similar results are also reported by Hamdeh et al. [16], where a 10 h milling in WC vials of $ZnFe_2O_4$ (initial $a = 0.845$ nm and $\delta = 0.21$) leads to an inversion parameter of 0.55 with a constant cell parameter.

3.2. Mössbauer study

Room temperature Mössbauer spectra for 3, 6 and 9 h of milling are plotted in Fig. 2a, along with the spectrum of a ceramic zinc ferrite.

At room temperature, ceramic zinc ferrite is characterized by a paramagnetic doublet (IS = 0.34 mm s^{-1}, $\Delta = 0.37$ mm s^{-1}). Below 10 K, it becomes antiferromagnetic and is then characterized by a sextet (IS = 0.47 mm s^{-1}, $\varepsilon = -0.016$ mm s^{-1}, $B = 51.2$ T) [17].

After 9 h of grinding, the spectrum can be fitted by a distribution of hyperfine fields with an average value of 24 T. The distribution (Fig. 2b) reveals two maxima, the first at low fields (around 7 T), and the second at high fields (around 36 T).

At this stage of the discussion, as a doublet alone is expected for $ZnFe_2O_4$, several hypotheses can be expressed concerning the shape of the Mössbauer spectrum.

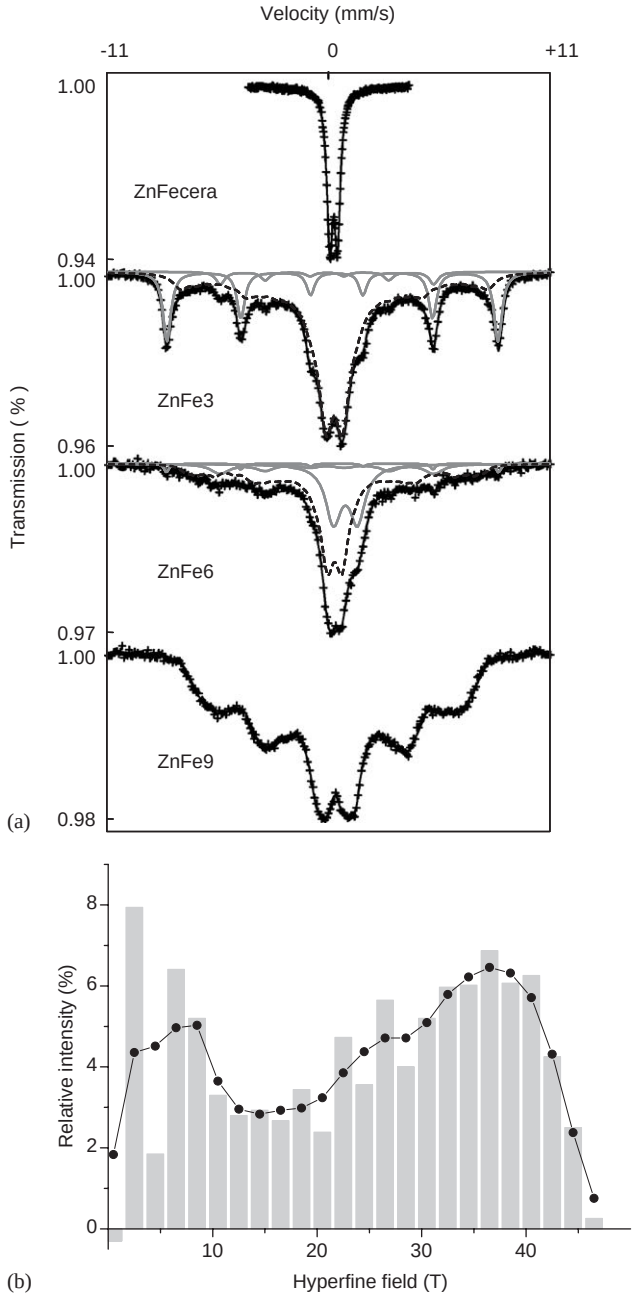

Fig. 2. (a) Mössbauer spectra of $ZnFe_2O_4$ ceramic and ball-milled ZnO–α-Fe_2O_3 mixture. Grey curves: contribution of α-Fe_2O_3, α-Fe or FeO. Dashed black curves: contribution of spinel phase. (b) Hyperfine field distribution corresponding to the ZnFe9 spectra. Column: experimental values. Points and curve: average values calculated with $A_{average} = (A_{n-1} + 2A_n + A_{n+1})/4$.

The spectrum, constituted of a magnetically ordered six-line pattern along with a paramagnetic doublet, can be explained on the basis of the presence of Fe ions with several environments (sites and neighbours), like in zinc-substituted magnetites [18].

The spectrum can also be typical of superparamagnetic relaxation with a distribution of relaxation times,

consequence of a particle size distribution in a magnetic sample. This effect is also observed and perfectly described in mechanosynthesized titanium ferrites by Guigue-Millot et al. [19] As $ZnFe_2O_4$ is know to be non-magnetic, the unexpected magnetism of this sample could be due to an inversion of the ferrite, commonly observed by mechanosynthesis [14–16]. In this case, the doublet arises from the superparamagnetic particles and the magnetic pattern results from the blocked particles. These two effects can be superimposed.

The existence of the only first effect (several environments for iron) is unlikely if we pay attention to the shape of X-ray diffraction lines. They have a super-Lorentzian shape, which is an evidence for a crystallite size distribution [20].

The Mössbauer spectrum of ZnFe3 and ZnFe6 are fitted taking into account the several phases observed by X-ray diffraction. The subspectrum due to spinel phase is fitted similarly to ZnFe9, along with a marked background curvature and a central doublet. The subspectrum due to wüstite-type phase is fitted with a doublet [21], α-Fe and α-Fe_2O_3 by sextets. Table 2 gives the hyperfine parameters the contibutions of each phase assuming that Lamb–Mössbauer factors are identical.

3.3. Discussion

X-ray diffraction and Mössbauer spectrometry results show that the milling of α-Fe_2O_3 + ZnO leads to the formation of an intermediate wüstite-type phase (containing some Fe(II)) along with a spinel phase, and at the end of the milling, to the formation of a pure spinel phase. Initially, iron is on the valency III in α-Fe_2O_3 and 0 in Fe coming from vials and balls. In order to explain the presence of iron on the valency II, two reactions may occur:

Oxidation of iron by the atmospheric oxygen

$$2Fe + O_2 \rightarrow 2FeO$$

Reduction of Fe(III).

The volume of the airtight vials is 80 mL, if the volume of the 5 balls is substracted, a volume of 14 mL of oxygen is available to oxidize iron, which leads to the formation of 1.16 mmol of Fe(II), representing about 4% of the total amount of iron in Fe_2O_3. Mössbauer analysis show that Fe(II) represents 25% of the total amount of Fe. Then, the hypothesis of a reduction of Fe(III) must also be considered to explain the presence of such an amount of Fe(II).

A change in the valency of iron has already been reported during the milling of α-Fe_2O_3 [22–24]. Kosmac et al. [23] have shown that hematite can be reduced by iron from vials or balls following the reaction:

$$Fe + \alpha\text{-}Fe_2O_3 \rightarrow Fe_3O_4. \quad (1)$$

The reduction may continue up to the obtention of FeO.

Kaczmarek et al. [24] suggest that iron-oxygen bonds are broken during the milling and oxygen is removed:

$$6Fe_2O_3 \rightarrow 4Fe_3O_4 + O_2. \quad (2)$$

In our case, a slight decompression when opening the mill containers after milling in air, indicating oxygen consumption, is noted. This fact allows to eliminate reaction (2).

Table 2
Hyperfine parameters and contributions of each phase for the different samples studied

Sample (%)	Phase	Isomer shift (mm s^{-1})	Quadrupole splitting or quadrupole shift (mm s^{-1})	Average field (T)	Contribution[a] (%)
ZnFe3	α-Fe_2O_3	0.38[b]	−0.21[b]	51.5[b]	20±2
	α-Fe	0[b]	0[b]	33[b]	5±1
	Spinel	0.36±0.01	0.00±0.01	16±1	75±5
ZnFe6	α-Fe_2O_3	0.38[b]	−0.21[b]	51.5[b]	2±1
	α-Fe	0[b]	0[b]	33[b]	10±3
	(Zn, Fe)O	0.94±0.01	1.19±0.01	—	25±5
	Spinel	0.38±0.01	0.00±0.01	16.3	63±5
ZnFe9	Spinel	0.40±0.01	−0.05±0.01	24.4±1	100
ZnFecera	$ZnFe_2O_4$	0.34±0.002	0.37±0.005	—	100
α-Fe_2O_3 9 h	α-Fe_2O_3	0.37±0.005	−0.095±0.005	50.9±0.1	100
3α-Fe_2O_3 + 1ZnO 9 h	α-Fe_2O_3	0.38[b]	−0.21[b]	51.5[b]	4±1
	α-Fe	0[b]	0[b]	33[b]	3±1
	Spinel *A* site	0.29±0.01	0.02±0.01	46.7±1	23±2
	Spinel *B* site	0.49±0.01	0.01±0.01	39.6±1	70±5

[a]Lamb–Mössbauer factors are supposed identical for each phase.
[b]Imposed.

Then, two phenomena have to be checked: if iron from milling tools is the origin of the reduction, and if this reduction concerns Fe^{3+} cations from α-Fe_2O_3 or from $ZnFe_2O_4$. For this purpose, millings of α-Fe_2O_3 and $ZnFe_2O_4$ separately have been made. Balls are weighed before and after milling, and XRD analysis is performed. Results are reported in Table 3.

X-ray diffraction patterns and Mössbauer spectra after milling of commercial hematite on the one hand, and of ceramic zinc ferrite on the other hand are represented, respectively, in Figs. 3 and 4.

In both cases, a broadening of the lines is noticed, and except iron, no FeO phase is detected. After the milling, zinc ferrite has a cell parameter of 0.8442 nm with crystallite size of 9.6 nm.

Mössbauer spectrum of milled α-Fe_2O_3 consists in one broadened sextet with hyperfine parameters ($DI = 0.37\,mm\,s^{-1}$, $\varepsilon = -0.095\,mm\,s^{-1}$, $B = 50.9\,T$) corresponding to unmilled hematite [25].

Mössbauer spectrum of milled $ZnFe_2O_4$ consists in a broadened doublet which does not allow to detect the presence of Fe(II). The broadening of the doublet is usually attributed to a change in the ions location, zinc leaving progressively tetrahedral sites to go into octahedral sites during milling [15,26,27], and to the intersublattice exchange interaction of the $Fe^{3+}[B]$–O^{2-}–$Fe^{3+}[B]$ allowed by the deformation of bond angles induced by milling [28].

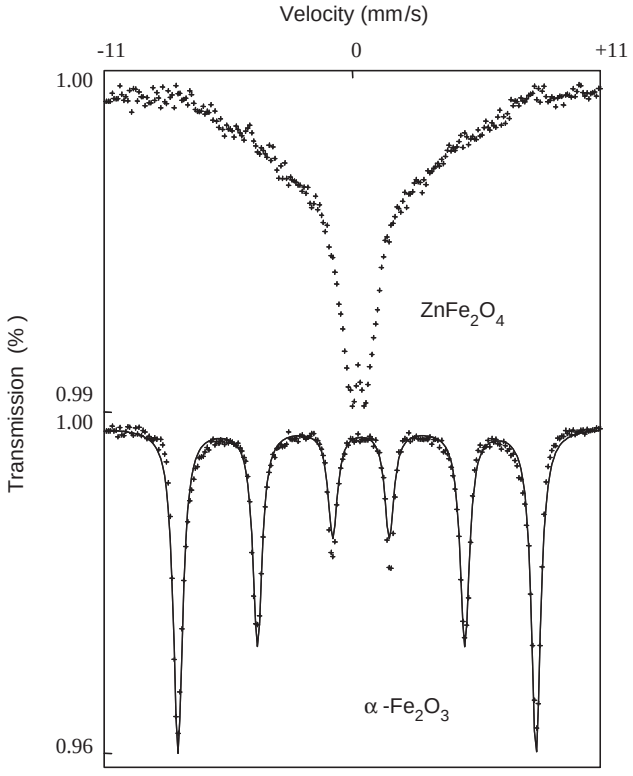

Fig. 4. Mössbauer spectra of ball-milled α-Fe_2O_3 (9 h) and $ZnFe_2O_4$ (6 h).

Table 3
Balls weight losses

Sample and milling time	Weight loss
α-Fe_2O_3 6 h/9 h	40 mg/50 mg
$ZnFe_2O_4$ 6 h	40 mg
1α-Fe_2O_3 + 1ZnO 9 h	110 mg
3α-Fe_2O_3 + 1ZnO 6 h	190 mg
$3ZnFe_2O_4$ + 1ZnO 6 h	80 mg
ZnO 6 h/9 h	−3 mg/−6 mg

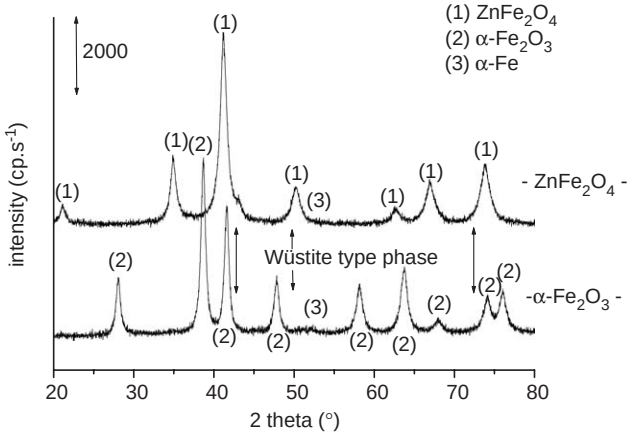

Fig. 3. X-ray powder diffraction patterns of ball-milled α-Fe_2O_3 (9 h) and $ZnFe_2O_4$ (6 h).

For $ZnFe_2O_4$ and α-Fe_2O_3 , as no reduction is observed neither by XRD nor by Mössbauer spectrometry, and as the balls weight losses are very low (around 40 mg) compared with this of α-Fe_2O_3 + ZnO (around 110 mg), we can assume that iron from balls (and probably from vials) is responsible for the reduction of hematite but this reduction seems to occur only in the presence of ZnO.

In order to show the influence of ZnO, α-Fe_2O_3 and $ZnFe_2O_4$ have been milled with zinc oxide (in a molar ratio 3 for 1) for 6 h.

For the mixture $3ZnFe_2O_4 + 1ZnO$, in spite of a high weight loss of the milling balls (see Table 3) which could be linked to a reduction, XRD analysis (Fig. 5) does not exhibit the presence of a wüstite-type solid solution. The only observed lines are these of the initial products and traces of metallic iron. Lines corresponding to ZnO are very broadened, and almost vanish. This indicates that, as for the milling of 1α-Fe_2O_3 + 1ZnO, zinc oxide becomes amorphous. The obtained zinc ferrite has a cell parameter of 0.8447 nm and a particle size of 8.2 nm.

Mössbauer spectrum is characterized by a broadened doublet (Fig. 6). However, this doublet is clearly less broadened than this of zinc ferrite milled without ZnO (Fig. 4). One can wonder if the inversion is less

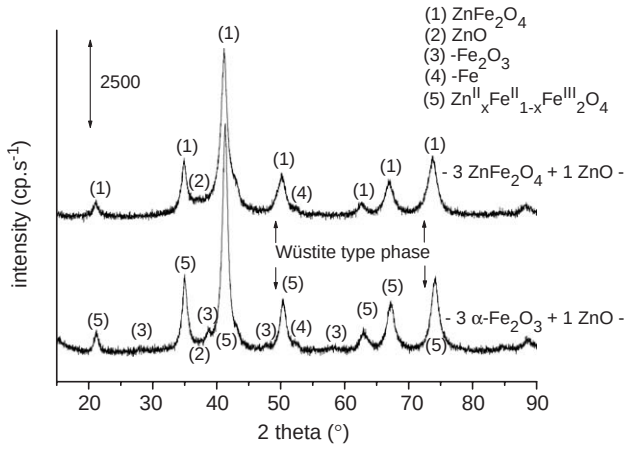

Fig. 5. X-ray powder diffraction patterns of ball-milled 3α-Fe_2O_3 + ZnO (6 h) and 3$ZnFe_2O_4$ + 1ZnO (6 h) mixtures.

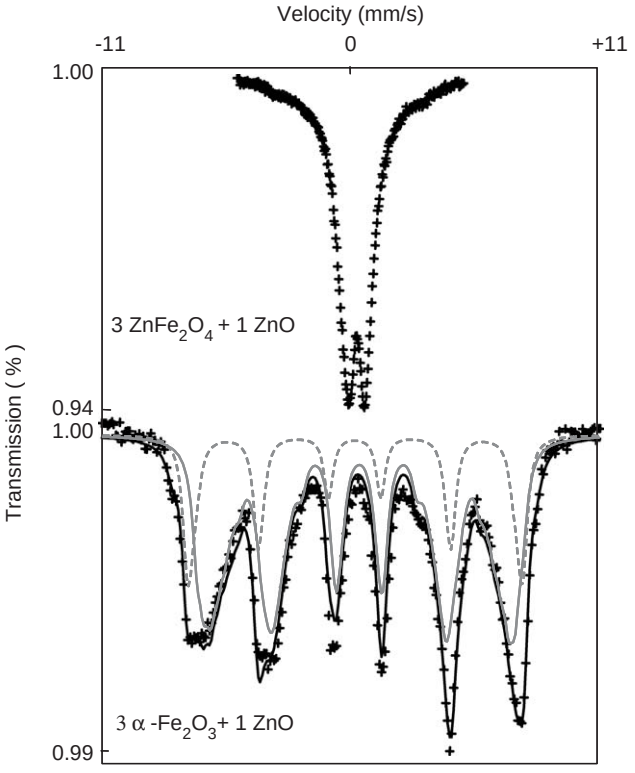

Fig. 6. Mössbauer spectra of ball-milled milled 3α-Fe_2O_3 + 1ZnO (6 h) and 3$ZnFe_2O_4$ + 1ZnO (6 h) mixtures. Dashed grey curve: contribution of iron in *A* site. Grey curve: contribution of iron in *B* site.

important, which seems to be true regarding the value of cell parameter, or if the broadening is reduced by the particle size ($ZnFe_2O_4$ milled alone: 9.6 nm, $ZnFe_2O_4$ milled with ZnO: 8.2 nm).

On the opposite, the milling of 3α-Fe_2O_3 + 1ZnO allows to put in evidence the reduction of Fe(III) into Fe(II). After the milling, which is accompanied by a high balls weight loss (190 mg, Table 3), an almost pure spinel phase is obtained, along with some traces of α-Fe_2O_3 and Fe (Fig. 5). The cell parameter of the spinel phase is 0.8414 nm, lower than this of milled zinc ferrite or this of ceramic zinc ferrite. Mössbauer spectrum (Fig. 6) is characterized by a sextet with broadened and dissymetrical lines. It can be fitted with two distributions of sextets corresponding to iron in *A* and in *B* sites, and with two sextets for α-Fe_2O_3 and α-Fe. Hyperfine parameters are $IS_A = 0.29\,mm\,s^{-1}$, average $B_A = 46.7\,T$ and $IS_B = 0.495\,mm\,s^{-1}$, average $B_B = 39.5\,T$, respectively, for iron in *A* and *B* sites.

Based on the value of the cell parameter, on the Mössbauer spectrum and on the results observed in literature [29,30], this spinel phase can be identified as a zinc-substituted magnetite $Zn^{II}_xFe^{II}_{(1-x)}Fe^{III}_2O_4$ with a substitution rate *x* close to 0.4–0.5.

The formation of this phase can be explained by the following redox reaction:

$$3\alpha\text{-}Fe_2O_3 + 1ZnO + 0.5Fe \rightarrow 2.5Zn_{0.4}Fe_{0.6}Fe_2O_4. \quad (3)$$

The formation of an intermediate wüstite-type phase is not observed, maybe it disappears very rapidly, leading to the spinel phase by reaction with α-Fe_2O_3.

Milling of α-Fe_2O_3 alone does not lead to reduction of Fe(III) whereas adding zinc oxide allows the obtaining of zinc-substituted magnetite. Then reduction of hematite is clearly favoured by the presence of ZnO.

In a first approach, the role of ZnO may be linked to its abrading capacity. If this one is higher compared to the other oxides, balls and vials would be highly damaged and small iron particles could be released in the mixture. Then, α-Fe_2O_3 could easily react with iron. Values of hardness for ZnO, $ZnFe_2O_4$ and αFe_2O_3 are, respectively, 4, 6 and 6 [31], which are not very different and reveal similar abrading capacities. Nevertheless, milling of ZnO for 6 and 12 h are performed. Values of weight losses are reported in Table 3, they are close to zero, even slightly negative (a small layer of zinc oxide remains at the surface of the balls). The balls are perfectly smooth, whereas for the other millings, some pits are observed. So, ZnO has no abrading capacity and it cannot make the reduction of Fe(III) easier.

Zinc oxide may form a solid solution with FeO, with a cubic structure and a cell parameter slightly increasing with the amount of zinc [21,32]. It seems that the solid solution between ZnO and FeO facilitates the reduction of Fe(III). Similar results have already been described in nickel, magnesium and manganese ferrites, where solid solutions of $Ni_{1-x}Fe_xO$, $Mg_{1-x}Fe_xO$ and $Mn_{1-x}Fe_xO$ are synthesized along with the spinel phase [33–35]. In the system Fe–Zn–O, such a solid solution is also observed in the case of milling α-Fe_2O_3 and ZnO, where the synthesis of the spinel phase is followed by its complete transformation into a wüstite-type phase [23]. This phase is also obtained in the case of milling magnetite with zinc (leading to zinc oxide and iron), as an intermediate state [36]. In all the cases, the nature of

the milling media (steel) plays an important role and is linked to the reduction phenomenon. Oxydoreduction reaction between α-Fe_2O_3 and Fe, associated with the presence of ZnO, may be written:

$$\alpha\text{-}Fe_2O_3 + ZnO + bFe \rightarrow (1-b)Zn_{0.4}Fe_{0.6}Fe_2O_4 + 4b(Fe_{0.75}Zn_{0.25})O. \quad (4)$$

With this reaction, we assume that after 6 h of milling, only a spinel phase and a wüstite-type phase are obtained. In this condition, the ratio Fe/Zn in the solid solution is imposed by the stoichiometric coefficients.

Two mechanisms are possible to explain the vanishing of the solid solution (Fe–Zn)O and the obtaining of an almost pure spinel phase: an insertion of Fe(II) in the spinel structure, or a replacement of Zn(II) by Fe(II) leading to the formation of ZnO. These two phenomena correspond to the following reactions:

$$(1-b)ZnFe_2O_4 + 4b(Fe_{0.75}Zn_{0.25})O \rightarrow Zn_xFe_{3-x}O_{4+\delta} \quad (5)$$

with $x = 3/(3+b)$ and $\delta = -4b/(3+b)$,

$$(1-b)ZnFe_2O_4 + 4b(Fe_{0.75}Zn_{0.25})O \rightarrow (1-b)Zn_x^{II}Fe_{(1-x)}^{II}Fe_2^{III}O_4 + 4bZnO \quad (6)$$

with $x = (1-4b)/(1-b)$.

Non-stoichiometric ferrites (i.e., deviating from the ideal formula AB_2O_4) may be written $M_xFe_{3-x}O_{4+\delta}$. M is a metal cation and δ is the deviation from stoichiometry [37,38]. If δ is positive, the spinel is cation deficient and exhibits some cation vacancies. On the opposite, if δ is negative, the spinel is oxygen deficient and may present either oxygen vacancies or interstitial cations in usually empty A or B sites.

Insertion of cations has been observed in several types of ferrites, in particular in lithium ferrites [39] or in copper ferrites [38]. Some non-stoichiometric Mn–Zn ferrites ($-0.04 < \delta < 0.015$) have been obtained [37], and according to the authors, they present some oxygen vacancies for negative δ and some cation vacancies for positive δ. Finally, Colombo et al. [40] have shown the existence of iron-rich magnetite $Fe_{3+w}O_4$ without indicating if it was a compound presenting oxygen vacancies or inserted cations. Anyway, for negative values of δ, the non-stoichiometry remains low (-0.04 [41], -0.015 [37]).

Chemical analysis of the sample ZnFe9a show that the molar ratio Fe/Zn is 2.3 (expected value: 2) and that the amount of chromium is 830 ppm. This contamination agrees with the balls composition in which majoritary impurities are chromium (1.5%) and carbon (1%). The excess of iron comes from the wear of the mill and the grinding balls and also from the reaction of Fe with Fe(III) giving Fe(II). If we try to calculate the formula of the different spinel phases with the two hypotheses, we can assume that if we do not want to take into account metallic iron, the molar ratio Fe/Zn is close to 2.1 ($b = 0.1$). For this value, the hypothesis of non-stoichiometry leads to the formula $Zn_{0.97}Fe_{2.03}O_{4-0.13}$, and the hypothesis of the replacement to the mixture $0.9\ Zn_{0.67}^{II}Fe_{0.33}^{II}Fe_2^{III}O_4 + 0.4ZnO$.

The obtaining of a non-stoichiometric ferrite is probable but it cannot, alone, explain the vanishing of the wüstite phase, because the value (–0.13) for δ is too high compared to the literature values.

Formation of zinc substituted magnetite has to be considered, which imposes that a fraction of zinc oxide does not react (Eq. (6)). With X-ray diffraction, it is difficult to identify unreacted zinc oxide which becomes amorphous during milling. Nevertheless, zinc oxide may be selectively dissolved by an ammonia solution, and then titrated by an EDTA solution [42]. By this method, it is found that about 3% in weight of the initial zinc oxide is unreacted after 9 h of milling. The formation of zinc substituted magnetite is then evidenced.

4. Conclusion

The spinel compound obtained after milling hematite and zincite is not a zinc ferrite containing only Fe^{3+} cations, but it is a zinc substituted magnetite. The presence of Fe(II) allows to explain the shape of the Mössbauer spectrum which is unusual for this type of milling. The appearance of this Fe(II)-containing phase is explained by a contamination due to iron from vials and balls, and by a redox reaction between iron and Fe(III) of hematite. This reaction only occurs in the presence of ZnO by the intermediate formation of a wüstite-type phase solid solution between ZnO and FeO. We have shown that the disappearance of this phase proceeds in the replacement of Zn^{2+} by Fe^{2+} inside the spinel phase, but this phase contains also probably an excess of Fe^{2+} ions (inserted cations or oxygen defects). Low-temperature Mössbauer experiments are planned in order to clarify this hypothesis.

References

[1] J. Smit, H.P.J. Wijn, Les ferrites, Bibliothèque Technique Philips Dunod, Paris, 1961.
[2] M.A. Ahmed, L. Alonso, J.M. Palacios, C. Cilleruelo, J.C. Abanades, Solid State Ionics 138 (2000) 51.
[3] N. Ikenaga, Y. Ohgaito, H. Matsushima, T. Suzuki, Fuel 83 (2004) 661.
[4] F.J. Burghart, W. Potzel, G.M. Kalvius, E. Schreier, G. Grosse, D.R. Noakes, W. Schafer, W. Kockelmann, S.J. Campbell, W.A. Kaczmarek, Physica B 289–290 (2000) 286.
[5] P. Druska, U. Steinike, V. Sepelak, J. Solid State Chem. 146 (1999) 13.
[6] A.E. Ermakov, E.E. Yurchikov, E.P. Elsukov, V.A. Barinov, Y.G. Chukalkin, Sov. Phys. Solid State 24 (1982).
[7] T. Verdier, V. Nivoix, M. Jean, B. Hannoyer, J. Mater. Sci. 39 (2004) 5151.

[8] P. Thompson, D.E. Cox, J.B. Hastings, J. Appl. Crystallogr. 20 (1987) 79.
[9] T. Roisnel, J. Rodriguez-Carvajal, Mater. Sci. Forum 378–381 (2001) 118.
[10] J.I. Langford, NIST Special Publication, vol. 846, 1992, p. 110.
[11] N. Lefelshtel, S. Nadiv, I.J. Lin, Y. Zimmels, Powder Technol. 20 (1978) 211.
[12] H.S.C. O'Neill, Eur. J. Mineral. 4 (1992) 571.
[13] V. Sepelak, K. Tkaova, V.V. Boldyrev, S. Wi[ss]mann, K.D. Becker, Physica B 234–236 (1997) 617.
[14] V. Sepelak, A.Y. Rogachev, U. Steinike, D.-C. Uecker, F. Krumeich, S. Wissmann, K.D. Becker, Mater. Sci. Forum 235–238 (1997) 139.
[15] F.S. Li, L. Wang, J.B. Wang, Q.G. Zhou, X.Z. Zhou, H.P. Kunkel, G. Williams, J. Magn. Magn. Mater. 268 (2004) 332.
[16] H.H. Hamdeh, J.C. Ho, S.A. Oliver, R.J. Willey, G. Oliveri, G. Busca, J. Appl. Phys. 81 (1997) 1851.
[17] F. Varret, A. Gerard, P. Imbert, Phys. Status Solidi 43 (1971) 723.
[18] C.M. Srivastava, S.N. Shringi, R.G. Srivastava, Phys. Rev. B 14 (1976) 2041.
[19] N. Guigue-Millot, S. Begin-Colin, Y. Champion, M.J. Hytch, G. Le Caër, P. Perriat, J. Solid State Chem. 170 (2003) 30.
[20] J. Plévert, D. Louër, J. Chim. Phys. 87 (1990) 1427.
[21] A.A. Lykasov, V.V. D'yachuk, G.I. Sergeev, Neorg. Mater. 21 (1985) 604.
[22] S. Linderoth, J.Z. Jiang, S. Morup, Mater. Sci. Forum 235–238 (1997) 205.
[23] T. Kosmac, T.H. Courtney, J. Mater. Res. 7 (1992) 1519.
[24] W.A. Kaczmarek, B.W. Ninham, IEEE Trans. Magn. 30 (1994) 732.
[25] N.N. Greenwood, T.C. Gibb, Mössbauer Spectroscopy, Chapman & Hall Ltd., London, 1971.
[26] K. Tkacova, V. Sepelak, N. Stevulova, V.V. Boldyrev, J. Solid State Chem. 123 (1996) 100.
[27] C.N. Chinnasamy, N.A.N. Ponpandian, K. Chattopadhyay, H. Guérault, J.M. Greneche, J. Phys.: Condens. Matter 12 (2000) 7795.
[28] V. Sepelak, K. Tkacova, V.V. Boldyrev, U. Steinike, Mater. Sci. Forum 228–231 (1996) 783.
[29] D.C. Dobson, J.W. Linnett, M.M. Rahman, J. Phys. Chem. Solids 31 (1970) 2727.
[30] T. Kanzaki, K. Kitayama, K. Shimokoshi, J. Am. Ceram. Soc. 76 (1993) 1491.
[31] D.R. Lide, CRC handbook of Chemistry and Physics, 80th ed, CRC Press, Boca Raton, 1999, pp. 4–139.
[32] J.M. Claude, M. Zanne, C. Gleitzer, J. Aubry, Mem. Sci. Rev. Met. 740 (1977) 229.
[33] M. Menzel, V. Sepelak, K.D. Becker, Solid State Ionics 141–142 (2001) 663.
[34] V. Sepelak, M. Menzel, K.D. Becker, F. Krumeich, J. Phys. Chem. B 106 (2002) 6672.
[35] F. Padella, C. Alvani, A.L. Barbera, G. Ennas, R. Liberatore, F. Varsano, Mater. Chem. Phys. 90 (2005) 172.
[36] L. Takacs, R.C. Reno, M. Pardavi-Horvath, Hyperfine Interactions 112 (1–4) (1998) 247.
[37] H. Inaba, J. Am. Ceram. Soc. 78 (1995) 2907.
[38] E. Kester, B. Gillot, C. Villette, P. Tailhades, A. Rousset, Thermochim. Acta 297 (1997) 71.
[39] C. Gleitzer, J.B. Goodenough, Structure and Bonding, vol. 61, Springer, Berlin, 1985.
[40] U. Colombo, F. Gazzarrini, G. Lanzavecchia, Mater. Sci. Eng. 2 (1967) 125.
[41] G. Bonsdorf, K. Schafer, K. Teske, H. Langbein, H. Ullmann, Solid State Ionics 110 (1998) 73.
[42] R. Furuichi, K. Tani, K. Kamada, T. Ishii, React. Solids 1 (1986) 309.